COMMUN. MATH. SCI.
Vol. 13, No. 5, pp. 1051–1074

STRANG SPLITTING METHODS FOR A QUASILINEAR SCHRÖDINGER EQUATION: CONVERGENCE, INSTABILITY, AND DYNAMICS*

JIANFENG LU† AND JEREMY L. MARZUOLA‡

Abstract. We study the Strang splitting scheme for quasilinear Schrödinger equations. We establish the convergence of the scheme for solutions with small initial data. We analyze the linear instability of the numerical scheme, which explains the numerical blow-up of large data solutions and connects to the analytical breakdown of regularity of solutions to quasilinear Schrödinger equations. Numerical tests are performed for a modified version of the superfluid thin film equation.

Key words. Strang splitting, quasilinear Schrödinger equations, convergence, stability, blow-up.

AMS subject classifications. 65M70, 35Q55.

1. Introduction

Consider a general quasilinear Schrödinger equation

$$iu_t = -\Delta u + uf(|u|^2) + ug'(|u|^2)\Delta g(|u|^2), \tag{1.1}$$

for $f,g:\mathbb{R}\to\mathbb{R}$. Such equations can be written as

$$\begin{cases} iu_t + a^{jk}(u,\nabla u)\partial_j\partial_k u = F(u,\nabla u), \quad u:\mathbb{R}\times\mathbb{R}^d\to\mathbb{C}^m \\ u(0,x) = u_0(x) \end{cases} \tag{1.2}$$

with small initial data in a space with relatively low Sobolev regularity. Note, quadratic quasilinear interactions can also be handled with some extra decay assumptions. Here

$$a:\mathbb{C}^m\times(\mathbb{C}^m)^d\to\mathbb{R}^{d\times d}, \qquad F:\mathbb{C}^m\times(\mathbb{C}^m)^d\to\mathbb{C}^m$$

are smooth functions which we will assume satisfy

$$a(y,z) = I_d + O(|y|^2+|z|^2), \qquad F(y,z) = O(|y|^3+|z|^3) \text{ near } (y,z)=(0,0).$$

Quasilinear equations of this form have arisen in several models. See [44] for a thorough list, but we mention here works related to the superfluid thin-film equation [35], modeling ultrashort pulse lasers [16, 17], and time dependent density functional theory

*Received: February 12, 2014; accepted (in revised form): October 28, 2014. Communicated by Shi Jin.
The first author was supported in part by the Alfred P. Sloan Foundation and by the National Science Foundation under grant number DMS-1312659. He would like to thank Weizhu Bao for helpful discussions. The second author was supported as a guest lecturer at Karlsruhe Institute of Technology in Summer 2013, as well as by NSF grant DMS-1312874, and wishes to especially thank his collaborators Jason Metcalfe and Daniel Tataru for introducing him to quasilinear Schrödinger theory. We also wish to thank the anonymous reviewers for many helpful comments that helped to improve the exposition in the manuscript. We thank Ludwig Gauckler also for pointing out an error in the convergence proof in an earlier version of the draft.

†Departments of Mathematics, Physics, and Chemistry, Duke University, Box 90320, Durham, NC 27708, USA (jianfeng@math.duke.edu).
‡Department of Mathematics, UNC-Chapel Hill, CB#3250 Phillips Hall, Chapel Hill, NC 27599, USA (marzuola@math.unc.edu).

[13]. The model we will consider here numerically equates to setting $g(s)=f(s)=s$, and hence

$$iu_t=-\Delta u+|u|^2u+u\Delta(|u|^2). \tag{1.3}$$

This is a pseudo-attractive version of the superfluid thin-film equation which is given by

$$iu_t=-\Delta u+|u|^2u-u\Delta(|u|^2) \tag{1.4}$$

and can be seen as a leading order contribution to the ultrashort pulse laser models from [16, 17]. Existence of solutions to quasilinear equations have been studied analytically in several cases; see [16, 17, 31, 32, 33, 39, 40, 44] and many others. The reason we choose to study (1.3) is that, while similar to (1.4) in that it is guaranteed to have small data local well-posedness from [40] and hence can be used to verify our numerical convergence results for general quasilinear models, the dynamics of (1.3) can lead to a breakdown of regularity due to a non-positive definite conserved energy. The model (1.4), on the other hand, has a positive energy quantity and, as a result, much more stable dynamics.

The nonlinear flow will allow interesting singularities to form in the evolution for large enough initial data. In particular, we observe blow-up at a particular amplitude threshold, but these singularities are representative of a breakdown of regularity in the higher derivatives and hence are not the standard self-similar style blow-up from the semilinear Schrödinger equation. Such a threshold was observed as an obstruction to local well-posedness using Nash–Moser type arguments in [36]. We show analytically that this mechanism for instability is inherited by the Strang splitting scheme through a rigorous convergence result and analysis of a finite frequency approximation. Moreover, we observe numerically that this threshold for ill-posedness arises in several different types of initial configurations and is rather robust. However, we note that this threshold is not the numerically observed sharp threshold for long-time well-posedness, as indeed the dynamics are able to drive nearby solutions to this critical amplitude. These features of (1.3) will be explored in Section 2.

Let us consider the nonlinear part of the equation

$$iv_t=vf(|v|^2)+vg'(|v|^2)\Delta g(|v|^2). \tag{1.5}$$

Taking the complex conjugate, we have

$$-i\overline{v}_t=\overline{v}f(|v|^2)+\overline{v}g'(|v|^2)\Delta g(|v|^2).$$

We calculate

$$\begin{aligned} i\partial_t|v|^2 &= i\overline{v}\partial_t v+iv\partial_t\overline{v}\\ &= |v|^2f(|v|^2)+|v|^2g'(|v|^2)\Delta g(|v|^2)\\ &\qquad -|v|^2f(|v|^2)-|v|^2g'(|v|^2)\Delta g(|v|^2)\\ &= 0, \end{aligned} \tag{1.6}$$

and hence, under the evolution (1.5), the amplitude is conserved. This will be a key property used to develop the numerical scheme.

Inspired by the above discussion, we consider a Strang splitting method for the quasilinear Schrödinger equation which is a composition of the exact flows of the differential equations

$$i\partial_t u=-\Delta u \tag{1.7}$$

and

$$i\partial_t u = uf(|u|^2) + ug'(|u|^2)\Delta g(|u|^2). \tag{1.8}$$

More concretely, we approximate $u(t_n)$ with $t_n = n\tau$ for a step size $\tau > 0$ by u_n via

$$\begin{aligned} u^-_{n+1/2} &= e^{\frac{i}{2}\tau\Delta} u_n; \\ u^+_{n+1/2} &= u^-_{n+1/2} \exp\Big(-i\tau\big(f(|u^-_{n+1/2}|^2) + g'(|u^-_{n+1/2}|^2)\Delta g(|u^-_{n+1/2}|^2)\big)\Big); \\ u_{n+1} &= e^{\frac{i}{2}\tau\Delta} u^+_{n+1/2}. \end{aligned} \tag{1.9}$$

We note that the scheme is explicit and symmetric thanks to the amplitude preserving property (1.6) of (1.5). One can use a Fourier pseudo-spectral method for the spatial discretization, and hence the flow $\exp(\frac{i}{2}\tau\Delta)$ can be efficiently calculated using the fast Fourier transform (FFT), and the flow (1.8) amounts to changing the phase of the solution on each mesh point.

Due to the advantage of being structure-preserving, the Strang splitting scheme [47] and higher order splitting schemes (e.g. [48, 53]) have been widely applied to a variety of nonlinear Schrödinger equations, mainly semilinear Schrödinger equations, modeling monochromatic light in nonlinear optics, Bose–Einstein condensates, as well as envelope solutions for surface wave trains in fluids. See for example [4, 5, 7, 8, 9, 10, 11, 14, 19, 21, 26, 27, 41, 42, 43, 46, 52]. While we focus on the strengths and weaknesses of applying the Strang splitting scheme for quasilinear Schrödinger equations, let us also mention that many other time discretization approaches to solve non-linear evolution equations have been developed, including Crank–Nicholson type schemes (see e.g. [45] and also [2] and [24] for applications in studying numerical blow-ups and nonlinear scattering), Magnus expansion approaches ([38] and also the recent review article [12]), exponential time-differencing schemes (see e.g. [15, 28]), implicit-explicit methods (see e.g. [6]), the comparison study in [49], and many others.

The convergence of splitting schemes for semilinear Schrödinger equations was analyzed in [18, 20, 25, 37, 46, 50]. In the present work, we extend the previous works to the quasilinear Schrödinger equation. The analysis follows the ideas in the seminal contribution by Lubich in [37] where the main tools are the calculus of Lie derivatives. We note that, however, there is a loss of derivatives associated with the nonlinear flow component in the middle step of the continuous Strang Splitting algorithm. This makes iteration of the approximation a challenge without taking smooth initial conditions. We will prove the convergence of the time-splitting method to the original evolution for the superfluid thin-film equation by first proving convergence to a mollified flow and then using convergence of the mollified flow to full continous quasi-linear problems. This allows us to do frequency cut-off dependent estimates. We will emphasize the regularity of the time flow, for which the behavior of the quasilinear Schrödinger equation is different from the semilinear ones. This is a Lie theoretic approach to the continuous time approximation and Sobolev-based well-posedness results of the second author with J. Metcalfe and D. Tataru in order to model small initial data solutions of finite time intervals [39, 40]. The scheme is symplectic and is stable within a range of parameters, motivated by the analysis in [40], where the analysis is done purely in Sobolev spaces H^s for s sufficiently large. In addition, the Strang splitting method converges in the order τ^2 for time step τ.

Moreover, we are able to extend a linear instability observed in a quasilinear Schrödinger equation in [36] to the numerical scheme used to approximate it, in a

Fréchet derivative sense, justifying the accuracy of a numerically observed blow-up. We study the dynamics of this blow-up solution using both Gaussian and plane-wave configurations of initial data to observe that the threshold for instability is not the sharp global well-posedness threshold for the equation and can indeed be reached through frequency dynamics on lower-amplitude solutions. This is not the standard blow-up through re-scaling of a nonlinear state but is a frequency instability of sorts that causes high frequencies to grow exponentially in a method akin to a backwards heat map.

The result is laid out as follows. We begin with a numerical study of the modified superfluid film equation in $1d$ (1.3) using the Strang splitting scheme (1.9). To analyze the convergence of the scheme, we discuss the mollification argument and prove the convergence of the mollified numerical scheme to the mollified flow for small data in Section 3 by using Lie theoretic results and necessary multilinear estimates. To understand the blow-up behavior observed for large enough data, we analyze the stability and instability of the scheme in Section 4. In Section 5, we discuss the regularity of the time flow of the quasilinear Schrödinger equation and the time-splitting scheme. In [36], an L^∞ threshold for local well-posedness was observed through use of Fréchet derivatives in a Nash–Moser scheme. We will show this similarly arises in analysis of exact plane-wave solutions on the torus using analysis similar to that of [52]. In order to establish the differentiability of the numerical solution with respect to time to sufficiently high accuracy, we rely on bounds in a much stronger topology in space. Finally, we tie together the numerical scheme and full quasilinear flow by addressing the convergence of mollified quasilinear equations to the full quasilinear flow in Section 6.

2. Numerical Results

To test the Strang splitting scheme (1.9) for quasilinear Schrödinger equations and numerically study the regularity breakdown, we consider the modified superfluid thin-film equation (see (1.3) and also [35, 44]) given by

$$iu_t + u_{xx} = |u|^2 u + (|u|^2)_{xx} u \tag{2.1}$$

on the domain $(-\pi,\pi]$ with periodic boundary condition. We have done similar computations for the ultrashort pulse laser equation as described in [16, 17], but no further interesting features of the numerical analysis arose, so we do not present them here for clarity of exposition.

2.1. Symmetric Gaussian initial condition Let us consider initial conditions given by

$$u(0,x) = ae^{-x^2/(2\sigma^2)} \tag{2.2}$$

on the domain $(-\pi,\pi]$ with periodic boundary condition. Here σ is the width and a is the amplitude of the Gaussian profile.

We calculate the solution up to time $T=\pi/4$ with parameters $a=1/5$ and $\sigma=1/5$ for the initial condition using a Fourier pseudo-spectral method with $N=256$ spatial grid points. To verify the second order accuracy of the time-splitting scheme, we choose different numbers of time steps and estimate the error by comparing the numerical solutions to a solution with $N_t=10^5$. The results in Table 2.1 and Figure 2.1 confirm the second order convergence.

Provided the solution remains in H^1, the PDE (2.1) conserves mass and energy given by

$$M(u) = \int |u|^2 \,\mathrm{d}x, \tag{2.3}$$

N_t	L^2-norm	H^1-seminorm
500	$1.6973e-06$	$4.7783e-04$
1000	$4.2241e-07$	$1.1878e-04$
2000	$1.0545e-07$	$2.9642e-05$
4000	$2.6323e-08$	$7.3990e-06$
8000	$6.5487e-09$	$1.8407e-06$

TABLE 2.1. *Numerical error of the time-splitting scheme for initial data* (2.2) *with* $a=1/5$ *and* $\sigma=1/5$ *at* $T=\pi/4$.

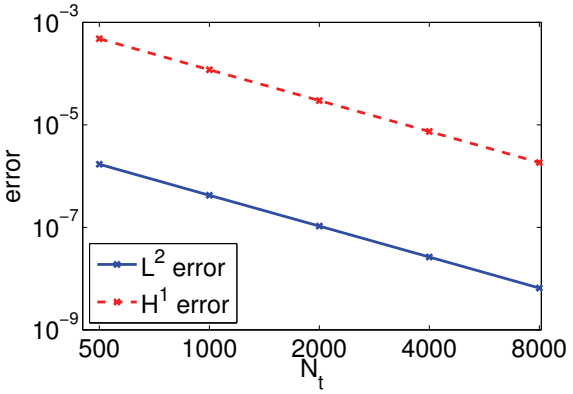

FIG. 2.1. *Log-log plot of the numerical error in Table 2.1 measured in* L^2 *norm and* H^1 *seminorm.*

$$E(u)=\frac{1}{2}\int |u_x|^2\,\mathrm{d}x+\frac{1}{4}\int |u|^4\,\mathrm{d}x-\frac{1}{4}\int |(|u|^2)_x|^2\,\mathrm{d}x. \tag{2.4}$$

The numerical scheme preserves the mass conservation law. While there is no energy conservation law [4, table 1], the energy is observed to remain numerically conserved with tiny deviation as shown in Figure 2.2.

Due to the nonlinearity of Equation (2.1), the problem becomes more stiff for initial conditions with larger amplitude or derivatives. For the family of Gaussian initial data (2.2), this means that one needs to increase a or reduce σ. We next consider the example with $a=0.625$, $\sigma=1/10$, and $T=\pi/4$. This problem is considerably more difficult than the one for the previous choice of parameters. We refine the spatial discretization to $N=512$ to resolve the oscillatory profile of the solution. The numerical error can be found in Table 2.2. We still observe second order accuracy, though, in this case, the time step size cannot be too large otherwise the numerical scheme becomes unstable.

We remark that to make the scheme more stable it is possible to apply Fourier spectrum truncation to eliminate spurious Fourier components of the numerical solution as introduced in [34]. At each time step, we set to zero all Fourier coefficients with amplitude below a certain threshold δ times the maximum amplitude of Fourier coefficients. In practice, for this example, we find the threshold $\delta=1e-3$ makes the scheme stable with $N_t=2000$ (recall that the solution is not stable for $N_t=10000$ without Fourier truncation). On the other hand, the filtering may introduce inconsistency in the numerical results.

To test the convergence with respect to the time step when a finer spatial mesh

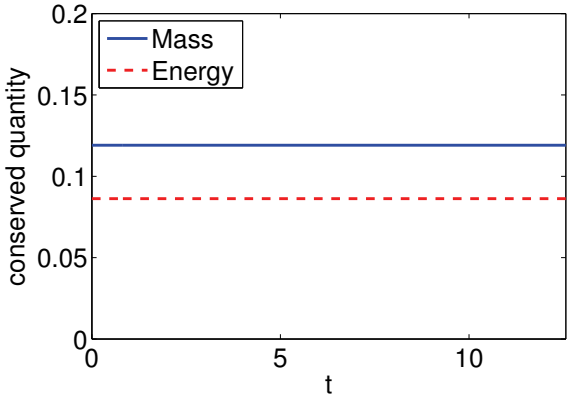

FIG. 2.2. *Mass and energy conservation for the numerical solution. The initial condition is given by* (2.2) *with* $a=1/5$ *and* $\sigma=1.5$. *The numerical solution is calculated up to time* $T=4\pi$ *and with* $N_t=32000$ *time steps. Energy and mass are recorded every* 100 *time steps.*

N_t	L^2-norm	H^1-seminorm
10000	unstable	
20000	$3.5573e-04$	$1.2775e-01$
40000	$3.0928e-04$	$5.1125e-02$
80000	$8.2591e-05$	$1.5832e-02$
160000	$1.9494e-05$	$4.1212e-03$
320000	$4.4489e-06$	$9.6345e-04$

TABLE 2.2. *Numerical error of the time-splitting scheme for initial data* (2.2) *with* $a=0.625$, $\sigma=1/10$, *and* $N=512$ *at* $T=\pi/4$. *The error is estimated by comparing the numerical solution with* $N_t=10^6$.

is used, we perform the same test with spatial discretization $N=1024$. The result is given in Table 2.3 and Figure 2.3 (left). A second order convergence rate is observed with the finer spatial mesh while the time step has to be smaller to ensure stability. The numerical conservation of energy and mass of the solution is shown in Figure 2.3 (right).

N_t	L^2-norm	H^1-seminorm
40000	unstable	
80000	$1.9672e-05$	$1.5458e-02$
160000	$6.8359e-06$	$4.2625e-03$
320000	$5.0287e-06$	$1.7278e-03$
640000	$1.1201e-06$	$5.4682e-04$
1280000	$2.6178e-07$	$1.4149e-04$
2560000	$6.1957e-08$	$3.4011e-05$

TABLE 2.3. *Numerical error of the time-splitting scheme for initial data* (2.2) *with* $a=0.625$, $\sigma=1/10$, *and* $N=1024$ *at* $T=\pi/4$. *The error is estimated by comparing the numerical solution with* $N_t=10240000$.

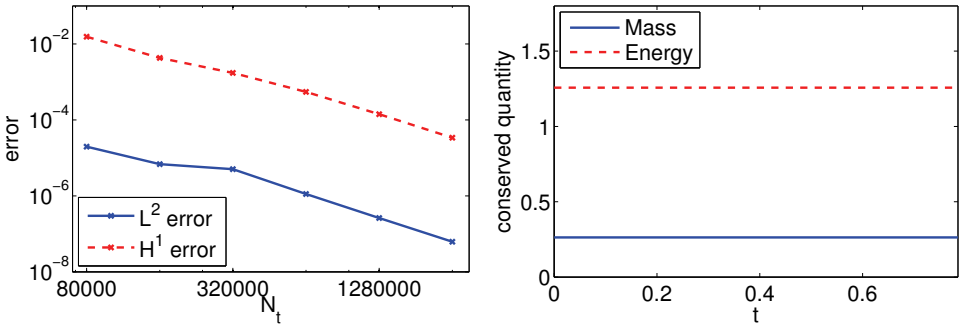

FIG. 2.3. *(Left) log-log plot of the numerical error in Table 2.3 measured in L^2 norm and H^1 seminorm. (Right) Mass and energy conservation for the numerical solution. The initial condition is given by* (2.2) *with $a=0.625$, $\sigma=1/10$, and $N=1024$. The numerical solution is calculated up to time $T=\pi/4$ and with $N_t=80000$ time steps. Energy and mass are recorded every* 1000 *time steps.*

If we further increase the amplitude of the initial condition, the numerical results indicate a "blow-up" behavior for the PDE. We increase the amplitude to $a=0.65$ while keeping $\sigma=1/10$. The numerical solution is calculated up to $T=5\times10^{-3}$. Figure 2.4 shows $\max|u(\cdot,t)|$ as a function of t for different choices of time step sizes. The sudden jump and exponential increase of the magnitude of maximum around $t=2.18\times10^{-3}$ indicates a numerical "blow-up" of the solution. Note that the onset point of the behavior does not depend on the choice of time step size indicating that this is not due to numerical instability of the time integration. Here we have chosen $N=4096$ spatial grid points. The blow-up behavior persists for further refinement of the spatial discretization.

To investigate more closely the above observed "blow-up", we study the solution around $x=0$ and the time when the "blow-up" occurs. We plot the absolute value of the solution in Figure 2.5. The numerical simulation indicates that the solution develops a "focusing peak" at $x=0$ with amplitude close to $\sqrt{2}/2$.

The numerical results suggest that the solution to the PDE becomes unstable for this family of initial conditions when the amplitude reaches about $\sqrt{2}/2$. To further confirm this, we compare the results for the initial condition with $a=0.625$ and $\sigma=1/10$; the solution stays below the amplitude of $\sqrt{2}/2$ as in Figure 2.6. Numerically, no blow-up is observed for $a=0.625$. The instability for large time step size is caused by pollution in the Fourier spectrum but not the intrinsic instability of solutions to the PDE.

2.2. Plane-wave initial conditions

The only exact solution we are aware of for the superfluid equation (2.1) is the family of wave trains:

$$u(x,t)=a\exp i(kx-\omega t). \tag{2.5}$$

This is a solution to (2.1) provided that

$$\omega=k^2+|a|^2. \tag{2.6}$$

Since $|u(x,t)|=|a|$ for the solution (2.5) at any x and t, the splitting error of the Strang splitting scheme vanishes since the potential commutes with the Δ operator.

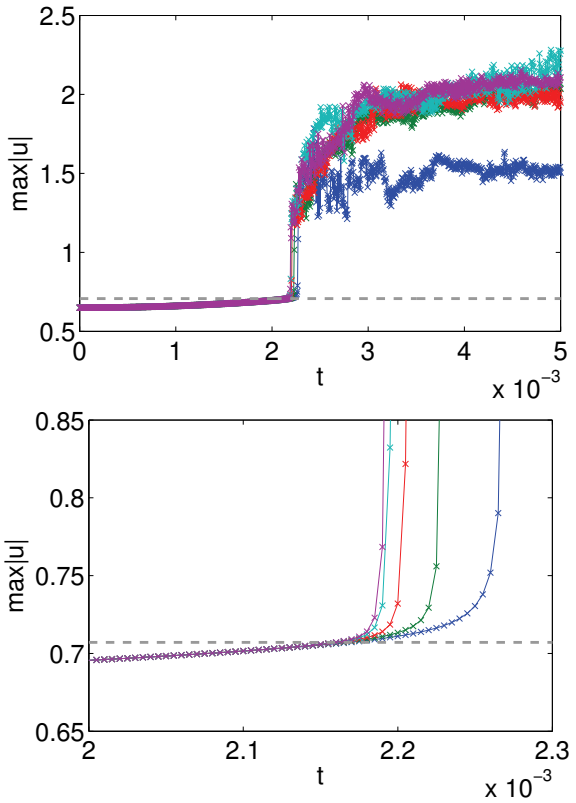

FIG. 2.4. $\max|u(\cdot,t)|$ *as a function of time for Gaussian initial conditions with* $a=0.65$ *and* $\sigma=1/10$. *Five time step sizes are taken corresponding to* $N_t=10000$, 20000, 40000, 80000, *and* 160000 *(blue, green, red, cyan, and purple curves) for total simulation time* $T=\pi$. *The bottom panel zooms in the region near the numerical blow-up. The dashed horizontal line indicates the level* $\sqrt{2}/2$.

We study the instability by adjusting the amplitude a of the initial data $u(x,0)=a\exp(ikx)$ of the solution (2.5). Figure 2.7 shows the simulation results for two solutions with initial conditions given by (2.5) with $a=\sqrt{2}/2-10^{-8}$ and $a=\sqrt{2}/2+10^{-8}$, respectively. Even though the amplitudes of the two solutions only differ by 2×10^{-8}, the behavior of the numerical solutions are completely different. While the numerical solution for the former is stable and accurate, the local truncation error kicks off instability in the latter case. This indicates again that $\sqrt{2}/2$ is the threshold of instability.

We also study multiple Fourier mode solutions to observe if non-local interactions can vary the blow-up profile. Hence, given a pseudospectral discretization scheme keeping the first N Fourier modes, we take initial data of the form

$$u(x,0)=a\sum_{j=1}\exp ik_jx \tag{2.7}$$

for $0\le k_1\le\cdots\le k_j\ll N$. The blow-up behavior of these solutions become more complicated; in particular, oscillations begin to factor around the blow-up after an initial exponential growth of the maximum amplitude (see Figure 2.8). However, it seems that generically $\sqrt{2}/2$ is still a threshold for blow-up.

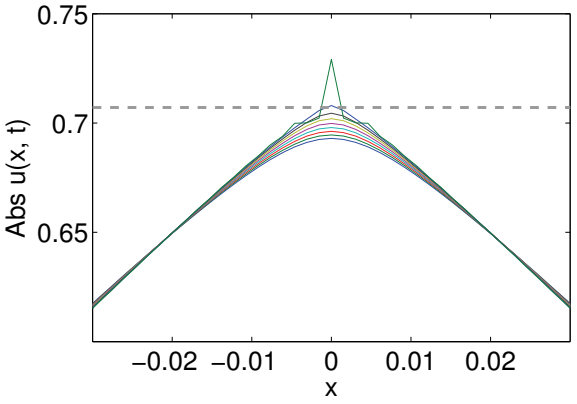

FIG. 2.5. *Snapshots of the absolute value of the numerical solutions around the numerical blow-up. The solution squeezes as time increases and leads to a blow-up. The reference horizontal line is plotted at the value* $\sqrt{2}/2$.

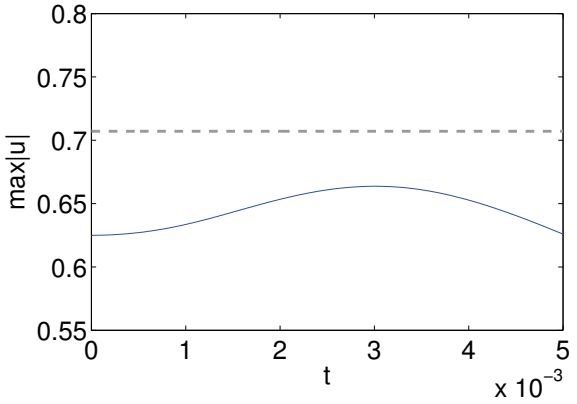

FIG. 2.6. *The maximum magnitude of* u *as a function of time for the initial condition with* $a=0.625$ *and* $\sigma=1/10$. *Compare with the quite different behavior in Figure 2.4.*

3. Convergence of the pseudo-spectral time-splitting scheme

In this section, we prove the convergence of a modified Strang splitting scheme to closely match the pseudospectral scheme used numerically for small data initial conditions. We suppose that the solution $u(t)$ to the modified superfluid thin film equation (2.1) in 1*d*is in H^7 for $0\leq t\leq T$ and wish to compare it to a Strang splitting flow defined so that an implicit frequency cut-off occurs at each stage of computation with the quasilinear nonlinearity. We show that the pseudo-spectral Strang splitting is well approximated by a mollified superfluid thin film equation. Since the analysis is somewhat dissimilar to that presented in this section related to the numerical algorithm, later in Section 6, we will compare the evolution of the mollified superfluid thin film equation to (2.1).

THEOREM 3.1. *The numerical solution* $u_{\epsilon,n}$, *given by the Strang splitting scheme with frequency cut-off* $|k|\leq\epsilon^{-1}$ *(defined below in* (3.17)*) with time step size* $\tau>0$ *on an*

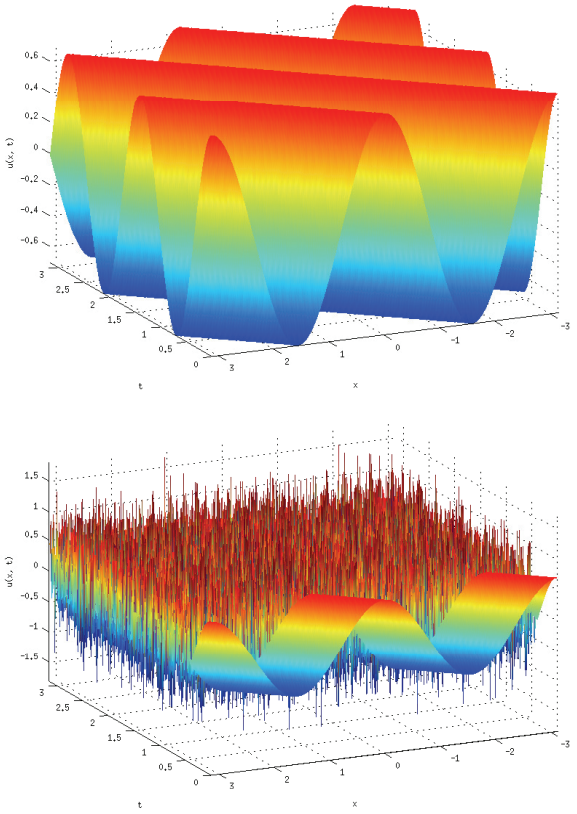

FIG. 2.7. *Numerical solution for* (2.5) *with* $a=\sqrt{2}/2-10^{-8}$ *and* $a=\sqrt{2}/2+10^{-8}$, *respectively. The solution to the PDE is unstable when the amplitude is larger than* $\sqrt{2}/2$.

interval of size $T=K\tau$ *for some* $K>0$, *has a second-order error bound in* H^1

$$\|u_{\epsilon,n}-u(t_0+\tau n)\|_{H^1}\leq C_1(m_7,\epsilon,T)\tau^2+C_2(m_4,T)\epsilon, \tag{3.1}$$

where

$$m_N=\max_{0\leq t\leq T}\|u(t)\|_{H^N}.$$

REMARK 3.1. *The small data local existence in* H^s *for the cubic quasilinear nonlinear terms is established in Marzuola–Metcalfe–Tataru [39, 40] (see also the works of Poppenberg [44], Kenig–Ponce–Vega, and Kenig–Ponce–Rolvung–Vega [29, 30, 31, 32, 33]). In particular, in the case of Equation* (1.3) *in dimension d,there exists a local in time solution in* H^σ *as long as* $\sigma>\frac{d+5}{2}$ *provided* u_0 *is sufficiently small. Therefore, the regularity assumption* $m_7<\infty$ *holds for sufficiently small data in* H^σ *for* σ *sufficiently large (and hence in* L^∞*). This is far from sharp, however, and much work must be done to explore the threshold between well-posedness and blow-up.*

REMARK 3.2. *The interplay between the* τ *and* ϵ *parameters arises only from the order* ϵ *bounds on the* H^1 *remainder of cutting the initial data off to frequencies below*

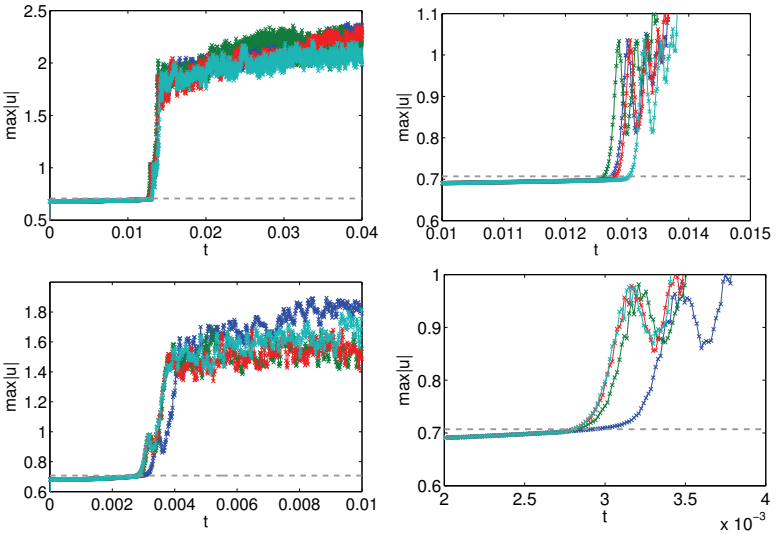

FIG. 2.8. $\max|u(\cdot,t)|$ *as a function of time for multiple Fourier mode initial conditions with* $a=0.65$ *and frequencies* $2,8$ *in the* 2*-mode setting (top), and* $2,8,14,20$ *in the* 4*-mode setting (bottom). Four time step sizes are taken corresponding to* $N_t=10000$, 20000, 40000, *and* 80000 *(blue, green, red, and cyan curves) for total simulation time* $T=0.15$. *The right panel zooms in the region near the numerical blow-up. The dashed horizontal line indicates the level* $\sqrt{2}/2$.

ϵ^{-1} *and evolving with a mollified Schrödinger flow. This will fully be addressed in Section 6 while below we compute the dependence with respect to* τ. *Indeed, the authors observed numerically that instability occurs when* τ *is taken too large. However, the work presented below represents the worst possible error bounds with relation to the effect of mollifying the equation which we think of as being related to the number of spatial grid points. Generically, the constant* C *in front of* τ^2 *can currently be quite large requiring very small* τ *to observe good convergence. In addition, the order of the* ϵ *dependent term in the convergence estimate can be improved by increasing the regularity of the initial data. The overall convergence estimates can be improved greatly by providing stronger regularity of the initial data, using smallness of the solution as required for the analysis in [39, 40], or, of course, shrinking the time interval* $[0,T]$ *as one must do for large data analysis of quasilinear problems.*

We will actually prove the result for arbitrary spatial dimension d,since the ideas are the same for any dimension. To start, we wish to establish the stability of the Strang splitting scheme with respect to a fixed time step. Before we begin, let us take

$$m_k=\|u(t)\|_{L^\infty H^k},\ k\leq\max\big(7,\frac{d+6}{2}+\eta\big), \tag{3.2}$$

for any $\eta>0$ such that u, the solution to (1.1) with small initial data, can be defined in H^k using [39, 40].

We can approximate the solution through the continuous time generators of the split step equations:

$$i\dot{\psi}=-\Delta\psi, \tag{3.3}$$

$$i\dot{\psi}=V[\psi]\psi, \tag{3.4}$$

where

$$V[\psi] = |\psi|^2 + \Delta(|\psi|^2). \tag{3.5}$$

The generators of the split step method can thus be described as exponential maps of the vector fields given by

$$\hat{T}(\psi) = i\Delta\psi, \tag{3.6}$$

$$\hat{V}(\psi) = -iV[\psi]\psi = -i[|\psi|^2 + \Delta(|\psi|^2)]\psi. \tag{3.7}$$

The key estimate we will require is of the type

$$\|\Delta(uv)w\|_{H^s} \leq C\|u\|_{H^{s+\frac{4+d}{2}+\eta}}\|v\|_{H^{s+\frac{4+d}{2}+\eta}}\|w\|_{H^s} \tag{3.8}$$

for $s > 0$ using the $L^\infty \times L^\infty \times L^2 \to L^2$ Hölder's inequality and the Sobolev embedding for L^∞. Note, the total loss of regularity on a given component of the multilinear estimates can be reduced with other estimates such as

$$\|\Delta(uv)w\|_{H^s} \leq C\|u\|_{H^{s+\frac{6+d}{3}}}\|v\|_{H^{s+\frac{6+d}{3}}}\|w\|_{H^{s+\frac{d}{3}}} \tag{3.9}$$

for $s \geq 0$ using $L^6 \times L^6 \times L^6 \to L^2$ Hölder's inequality and the Sobolev embedding for L^6 as well as moving to L^p based spaces and applying the techniques of Strichartz estimates, etc. However, we will use (3.8) throughout since in the mollification the loss in ϵ will be scale invariant for any choice, plus it turns out to be beneficial to have one component remain free of derivatives to take advantage of the short time gains we will observe in the Lie Theory.

Before computing Lie derivatives, we want to understand the stability of the evolution generated by $\hat{V}$. To do this, we study

$$i\dot{\nu} = V[\psi]\nu, \quad \nu(0) = \psi. \tag{3.10}$$

For ψ sufficiently regular, it is possible to show that the evolution varies continuously with the choice of initial data in a weak topology. In particular, given

$$i\dot{\nu} = V[\psi]\nu, \quad \nu(0) = \psi,$$
$$i\dot{\mu} = V[\phi]\mu, \quad \mu(0) = \phi,$$

by looking at the difference of these two evolutions, expanding $V[\phi]\mu - V[\psi]\nu = (V[\phi] - V[\psi])\mu - V[\psi](\nu - \mu)$, and applying (3.8), we have

$$\|\mu(t) - \nu(t)\|_{H^s} \leq \|\psi - \phi\|_{H^s} + C_1 t\|\psi - \phi\|_{H^{s+\frac{d+4}{2}+\eta}} + C_2\int_0^t \|\mu(s) - \nu(s)\|_{H^s} \tag{3.11}$$

for any $\eta > 0$ and $s > \frac{d+4}{2}$ chosen sufficiently large to control the evolution where C_1, C_2 both depend upon $M_s = \max_{0\leq t\leq T}\{\|\phi\|_{H^s}, \|\psi\|_{H^s}\}$. As a result, a Gronwall type argument shows

$$\|\mu(t) - \nu(t)\|_{H^s} \leq e^{C_0\tau}\|\psi - \phi\|_{H^{s+\frac{d+5}{2}}}, \tag{3.12}$$

where C_0 depends upon m_k.

Unfortunately, the above estimate comes with a regularity loss (it requires higher Sobolev on the previous time step). As a result, it is not sufficient to provide an

error estimate unless we assume that the solution is smooth.[1] This can be dealt with for certain types of derivative nonlinearities that are not quasilinear; see for instance [23]. See also [3] for a recent analytic treatment of convergence of mollified derivative Schrödinger equations on the torus.

To resolve the issue, let us introduce a mollified equation given by

$$iu_{\epsilon,t}+u_{\epsilon,xx}=G_\epsilon*[|u_\epsilon|^2u_\epsilon]+G_\epsilon*[\Delta(|u_\epsilon|^2)u_\epsilon], \tag{3.13}$$

where G_ϵ is a smooth, compactly supported mollifier that cuts off the high frequency terms of the evolution such that if $u\in H^s$ we have

$$\|G_\epsilon u-u\|_{H^{s-1}}\le C\epsilon\|u\|_{H^s} \quad \text{and} \tag{3.14}$$

$$\|G_\epsilon u\|_{H^{s+1}}\le C\epsilon^{-1}\|G_\epsilon u\|_{H^s}. \tag{3.15}$$

Note, G_ϵ is a standard, smooth, Littlewood–Paley cut-off in frequency space at the frequency $\mathcal{O}(1/\epsilon)$. See for instance [3, Section 2] for the construction of such a mollifier.

As will be shown in Section 6, the mollified flow and the original flow are close for small initial data using the frequency envelope type arguments of [39, 40] that prove the high frequency terms remain small over the order 1 lifespan. If $\|u_0\|_{H^{s+3}}$ is small, then

$$\|u_\epsilon(t)-u(t)\|_{L^\infty H^s}\le C\epsilon. \tag{3.16}$$

Hence, we will analyze the Strang splitting on the mollified flow (3.13). From the point of view of the fully discretized flow, e.g. with pseudospectral method, the inclusion of a frequency cut-off is also quite natural. Actually, the numerical result in Section 2 can be understood as discretizations of (3.13) since the number of Fourier modes N is fixed as the time step is reduced, and the numerical solution is compared to that with a tiny time step (but fixed spatial resolution).

For the mollified flow, the Strang splitting scheme converges with second order error, albeit with a possibly large constant depending upon the regularity of the initial data.

PROPOSITION 3.2. *Consider the numerical solutions $u_{\epsilon,n}$ given by the Strang splitting scheme on the mollified equation:*

$$\begin{aligned}
&u^-_{\epsilon,n+1/2}=e^{\frac{i}{2}\tau\Delta}u_{\epsilon,n};\\
&u^+_{\epsilon,n+1/2}=u^-_{\epsilon,n+1/2}\exp\big(-i\tau G_\epsilon(|u^-_{\epsilon,n+1/2}|^2+\Delta|u^-_{\epsilon,n+1/2}|^2)\big);\\
&u_{\epsilon,n+1}=e^{\frac{i}{2}\tau\Delta}(G_\epsilon u^+_{\epsilon,n+1/2}).
\end{aligned} \tag{3.17}$$

The numerical solution converges to the solution of the mollified equation as $\tau\to 0$ provided that τ is sufficiently small:

$$\|u_{\epsilon,n}-u_\epsilon(t_0+\tau n)\|_{H^1}\le C(m_7,\epsilon,T)\tau^2. \tag{3.18}$$

REMARK 3.3. *In the mollified Strang splitting algorithm above, it is possible that there is small loss of L^2 norm conservation in the splitting scheme due to cutting off at high-frequency in the third step of the method. However, we note that in the pseudo-spectral*

[1] The authors thank Ludwig Gauckler for pointing this out which fixes an error in an earlier version of the argument.

method the evaluation of the product of the nonlinear phase and $u^-_{\epsilon,n+1/2}$ *in the middle step is done completely on the spatial side which already includes essentially a cut-off below a given frequency scale related to the grid spacing. Hence, in the fully discrete implementation, the* L^2 *norm is actually conserved.*

REMARK 3.4. *Theorem 3.1 follows from the above remark and Proposition 6.1 in Section 6.*

Proof. The convergence proof follows a Lie theoretic idea of Lubich [37] for semilinear nonlinear Schrödinger equations.

Denote

$$V_\epsilon[\psi] = G_\epsilon * [|\psi|^2] + G_\epsilon * [\Delta(|\psi|^2)]$$

and consider two flows given by

$$\begin{aligned} i\dot{\nu} &= V_\epsilon[\psi]\nu, \quad \nu(0) = \psi; \\ i\dot{\mu} &= V_\epsilon[\phi]\mu, \quad \mu(0) = \phi. \end{aligned}$$

Using essentially the same calculation leading to (3.11), we arrive at

$$\begin{aligned} \|\mu(t)-\nu(t)\|_{H^s} &\le \|\psi-\phi\|_{H^s} + C_1 t \|G_\epsilon * (\psi-\phi)\|_{H^{s+\frac{d+4}{2}+\eta}} + C_2 \int_0^t \|\mu(s)-\nu(s)\|_{H^s} \\ &\le \|\psi-\phi\|_{H^s} + C_1 t \epsilon^{-(d+4)/2-\eta} \|\psi-\phi\|_{H^s} + C_2 \int_0^t \|\mu(s)-\nu(s)\|_{H^s}. \end{aligned} \tag{3.19}$$

Note that in the last step we have used an inverse inequality thanks to the frequency cut-off in G_ϵ. Therefore, a Gronwall type argument gives

$$\|\mu(t)-\nu(t)\|_{H^s} \le e^{C_0(\epsilon)t} \|\psi-\phi\|_{H^s}, \tag{3.20}$$

where C_0 depends on m_k, for $k = s + \frac{d}{2} + 2 + \eta$, in terms of the size of the data as well as the ϵ in the mollifier.

Now, to compare the full evolution to the mollified split-step method, we must compute the Lie commutators between generating vector fields. As mollification will only reduce norms, below, for simplicity, we work with continuous versions of the Strang splitting flow. However, in the discussion below, the reader should keep in mind the case when $V = V_\epsilon$. We observe

$$\begin{aligned} [\hat{T},\hat{V}]\psi = &\Delta\left(|\psi|^2\psi - \Delta(|\psi|^2)\psi\right) \\ &- \left[2\Delta\psi(\bar{\psi}\psi - \psi^2\overline{\Delta\psi})\right] \\ &- \left[\Delta(\Delta\psi\bar{\psi})\psi - \Delta(\psi\overline{\Delta\psi})\psi + \Delta(|\psi|^2)\Delta\psi\right]. \end{aligned} \tag{3.21}$$

Hence,

$$\|[\hat{T},\hat{V}](\psi)\|_{H^1} \le C\|\psi\|^3_{H^{\max(5,\frac{4+d}{2}+)}}. \tag{3.22}$$

In addition, we then can easily compute

$$\|[\hat{T},[\hat{T},\hat{V}]](\psi)\|_{H^1} \le C\|\psi\|^3_{H^{\max(7,\frac{6+d}{2}+)}}. \tag{3.23}$$

Setting the vector field $\hat{H} = \hat{T} + \hat{V}$, the underlying idea is that the evolution of the full quasilinear Schrödinger equation, given by the exact evolution

$$\psi(\tau) = \exp(\tau D_H)\,\mathrm{Id}(\psi_0) \tag{3.24}$$

when well defined (by making the initial condition sufficiently high regularity), can be compared through a double Duhamel expansion to the split-step generator

$$\psi_{SS}(\tau)=\exp(\frac{1}{2}\tau D_T)\exp(\tau D_V)\exp(\frac{1}{2}\tau D_T)\mathrm{Id}(\psi_0), \tag{3.25}$$

the error terms of which can be written using the Lie commutators. Since the frequency mollifier we wish to include in the pseudo-spectral implementation commutes with the left-most $\exp(\frac{1}{2}\tau D_T)$ iteration, we again proceed with the continuous estimates and recognize that, in the end, we will cut-off in frequency which only reduces norms.

Indeed, the error estimates come from successive application of the quadrature first order error formula

$$\tau f(\frac{1}{2}\tau)-\int_0^\tau f(s)\,\mathrm{d}s=\tau^2\int_0^1\kappa_1(\theta)f'(\theta\tau)\,\mathrm{d}\theta \tag{3.26}$$

and the second-order error formula

$$\tau f(\frac{1}{2}\tau)-\int_0^\tau f(s)\,\mathrm{d}s=\tau^3\int_0^1\kappa_2(\theta)f''(\theta\tau)\,\mathrm{d}\theta, \tag{3.27}$$

where $\kappa_1(\theta)$ and $\kappa_2(\theta)$ are the Peano kernels for the midpoint rule,

$$f(s)=\exp((\tau-s)D_T)D_V\exp(sD_T)\mathrm{Id}(\psi_0),$$

and hence

$$\begin{aligned}f'(s)&=e^{is\Delta}[\hat{T},\hat{V}]e^{i(\tau-s)\Delta}\psi_0,\\ f''(s)&=e^{is\Delta}[\hat{T},[\hat{T},\hat{V}]]e^{i(\tau-s)\Delta}\psi_0.\end{aligned}$$

Note, the Peano kernels are defined as the integral kernels of the linear transformation

$$L:C^{k+1}[0,T]\to\mathbb{R}$$

such that

$$L(f)=f-\sum_{j=0}^{k}\frac{f^{(j)}(0)}{j!}T^j=\frac{1}{k!}\int_0^T\kappa_k(s)f^{(k+1)}(s)ds.$$

Hence we observe that, using the mid-point rule, the $f'(t/2)$ term vanishes explaining why there is not a quadratic term in (3.27), though the expressions (3.26) and (3.27) can still vary due to the nature of the error term expansions in both cases. Hence, it is essential for the argument below we can prove that for our approximation we have $f(s)\in C^3$ which strongly relates to the analyticity of the linear Schrödinger evolution kernel in the Strang splitting scheme since, in particular, a generic quasilinear Schrödinger flow cannot be shown to be more than C^0 by the purely dispersive techniques in [39, 40]. We will come back to this in more detail in Section 5.

Applying (3.24), (3.25), (3.22), (3.23), and (3.11) in succession, as in [37], gives

$$\|u_{n,\epsilon}-u_\epsilon(t_n)\|_{H^1}\le C(m_{K_0},\epsilon,T)\tau^2 \tag{3.28}$$

for $t_n=n\tau\le T$ and $K_0=\max(7,\frac{d+6}{2}+\eta)$ for the mollified flow when τ is small compared to ϵ.

From the continuous point of view, in order to obtain the τ^2 convergence here, it is important to compute the double commutator bound leading to (3.25) in order to expand out to 3rd order in the Lie derivatives. However, we note the same quadratic convergence would hold in L^2 with only $K_0 = \max(5, \frac{d+5}{2} + \eta)$ as then the double Duhamel commutator would not be required and we would be mostly restricted by the well-posedness threshold for (1.1). □

REMARK 3.5. *So far we have considered the convergence of the time-splitting flow to the flow of the original PDE. We further discretize the spatial degree of freedom using a Fourier pseudo-spectral method. The convergence of the fully discretized scheme follows if we can show that the fully discretized scheme converges to the time-splitting flow, though this is beyond the scope of our aim in this work. See, for instance, [20, 46, 51, 22] for analysis of the fully discretized scheme for semilinear Schrödinger equations. The importance of analysis of the fully discretized scheme moving forward is quite clear from the necessity of mollifying the Strang splitting algorithm here. The authors hope to consider this more carefully in future work.*

REMARK 3.6. *Since the mollified equation becomes effectively semi-linear, one could pose the question as to whether or not much of the quasilinear analysis on the continuous problem presented here is necessary for proof of convergence or if the semilinear tools could be applied. Actually, one can apply the semilinear techniques to the mollified continuous flow, however the existence time of the model for the initial data would become exponentially small depending upon the ϵ threshold in the frequency cut-off. Hence, using the quasilinear flow estimates is quite important in order to get uniform control on the continuous mollified problem over the time 1 existence interval for the full continuous problem. However, in using Strang-Splitting methods with the derivative part of the nonlinearity in the potential step, we are locally treating the evolution of this term as a semilinear approximation which means we must figure out how to uniformly apply the ideas of [37] and why the time step τ must be taken to be short enough to allow uniform errors with relation to the mollification.*

4. Stability and instability of the numerical scheme

As discussed in Section 2, for large data, we observe blow-up behavior in the numerical study. In this section, we will investigate the numerical instability of the scheme which will shed some light on the blow-up behavior.

4.1. Linear stability analysis for wave train

For the uniform wave trains solution (2.5), we study the stability for perturbations around the solution. Consider a perturbed solution of the form

$$u(x,t) = u_0(x,t)(1+\varepsilon(x,t)), \tag{4.1}$$

where u_0 is the plane-wave solution $ae^{i(kx-\omega t)}$ and $|\varepsilon|^2 \ll 1$. For the leading order, we get

$$i\varepsilon_t + 2ik\varepsilon_x + \varepsilon_{xx} = |a|^2(\varepsilon+\bar{\varepsilon}) + |a|^2(\varepsilon+\bar{\varepsilon})_{xx}. \tag{4.2}$$

Let us expand ε in a Fourier series (with $\xi_n = n$ for ε periodic on $[0,2\pi]$):

$$\varepsilon(x,t) = \sum_{n=-\infty}^{\infty} \widehat{\varepsilon}_n(t)\exp(i\xi_n x). \tag{4.3}$$

The equation of ε can then be written as a system of ODEs,

$$\frac{\mathrm{d}}{\mathrm{d}t}\begin{pmatrix} \widehat{\varepsilon}_n \\ \widehat{\bar{\varepsilon}}_{-n} \end{pmatrix} = G_n \begin{pmatrix} \widehat{\varepsilon}_n \\ \widehat{\bar{\varepsilon}}_{-n} \end{pmatrix}, \tag{4.4}$$

where

$$G_n = i\begin{pmatrix} -2k\xi_n - |\xi_n|^2 - |a|^2 + |a|^2|\xi_n|^2 & -|a|^2 + |a|^2|\xi_n|^2 \\ |a|^2 - |a|^2|\xi_n|^2 & -2k\xi_n + |\xi_n|^2 + |a|^2 - |a|^2|\xi_n|^2 \end{pmatrix}. \tag{4.5}$$

The eigenvalue of G_n, λ_n, is given by

$$\lambda_n = -2ik\xi_n \pm |\xi_n|\sqrt{-|\xi_n|^2 - 2|a|^2 + 2|a|^2|\xi_n|^2}. \tag{4.6}$$

The solution becomes unstable if one of the eigenvalues has a positive real part or, equivalently,

$$2|a|^2|\xi_n|^2 - 2|a|^2 - |\xi_n|^2 > 0. \tag{4.7}$$

A sufficient condition for stability is

$$|a| \le \sqrt{2}/2. \tag{4.8}$$

Note that the stability threshold $\sqrt{2}/2$ agrees with the numerical observations in Section 2.

4.2. Linear Stability Analysis for the Strang splitting algorithm

To study the stability of general initial data, where an explicit solution is not available, we linearize around a solution to (1.1). Locally, the linear instability is essentially equivalent to the plane-wave instability observed in Section 2.2 and analyzed in the previous subsection. The key observation is that the instability occurs for all k. This has been done in [36, Equation (8)] where one observes that perturbation around a solution $u = w + z$ leads to

$$z_t = a[M_w \Delta z + G_w \nabla z + H_w z] + f(t), \quad z(0) = g, \tag{4.9}$$

where, for $w = w_1 + iw_2$, we observe

$$M_w = \begin{bmatrix} 2w_1w_2 & 2w_2^2 - 1 \\ 1 - 2w_1^2 & -2w_1w_2 \end{bmatrix}$$

which has determinant $1 - 2|w|^2$. The matrix functions G_w and H_w come from the linearization and will be expressed in full in (4.10) below. Using this linearization and a Fréchet based iteration argument in the space H^∞, the authors then show local well-posedness for small data solutions to equations of the form (1.1).

To understand the instability of the numerical scheme, we linearize the discretized Strang splitting algorithm and show that the linear instability threshold in the continuous problem exists in the discretized version as well. Letting $u = w + z$ for some solution w of (1.4), and generally writing $h(x,t) = h_1(x,t) + ih_2(x,t)$ for any complex function h, we have that the linearized continuous PDE (4.9) takes the form (see also [36])

$$\begin{aligned} \begin{bmatrix} z_1 \\ z_2 \end{bmatrix}_t &= \begin{bmatrix} 2w_1w_2\Delta & (2w_2^2 - 1)\Delta \\ (1 - 2w_1^2)\Delta & -2w_1w_2\Delta \end{bmatrix} \begin{bmatrix} z_1 \\ z_2 \end{bmatrix} + \begin{bmatrix} 2w_2^2 + 2w_1w_2 & w_1^2 + w_2^2 \\ -[3w_1^2 + w_2^2] & -2w_1w_2 \end{bmatrix} \begin{bmatrix} z_1 \\ z_2 \end{bmatrix} \\ &+ \begin{bmatrix} 4w_2\nabla w_1 \cdot \nabla & 4w_2\nabla w_2 \cdot \nabla \\ -[4w_1\nabla w_1 \cdot \nabla] & -[4w_1\nabla w_2 \cdot \nabla] \end{bmatrix} \begin{bmatrix} z_1 \\ z_2 \end{bmatrix} \\ &+ \begin{bmatrix} 2w_2\Delta w_1 & \sum_{j=1}^2 2\nabla \cdot (w_j \nabla w_j)) + 2w_2\Delta w_2 \\ -\left[\sum_{j=1}^2 2\nabla \cdot (w_j \nabla w_j) + 2w_1\Delta w_1\right] & -2w_1\Delta w_2 \end{bmatrix} \begin{bmatrix} z_1 \\ z_2 \end{bmatrix}. \end{aligned} \tag{4.10}$$

We then have

$$M_w = \begin{bmatrix} 2w_1w_2 & 2w_2^2-1 \\ 1-2w_1^2 & -2w_1w_2 \end{bmatrix}, \quad G_w = \begin{bmatrix} 4w_2\nabla w_1^T & 4w_2\nabla w_2^T \\ -4w_1\nabla w_1^T & -4w_1\nabla w_2^T \end{bmatrix},$$

$$H_w = \begin{bmatrix} 2w_2^2+2w_1w_2+2w_2\Delta w_1 & H_{12} \\ -H_{21} & -[2w_1w_2+2w_1\Delta w_2] \end{bmatrix},$$

where

$$H_{12} = w_1^2+w_2^2+2w_1\Delta w_1+2\nabla w_1\cdot\nabla w_1+4w_2\Delta w_2+2\nabla w_2\cdot\nabla w_2,$$
$$H_{21} = 3w_1^2+w_2^2+4w_1\Delta w_1+2\nabla w_1\cdot\nabla w_1+2w_2\Delta w_2+2\nabla w_2\cdot\nabla w_2+4w_1\nabla w_1.$$

We wish to compare the linearization of the full PDE to the discretized linearization of the form

$$\begin{aligned} z^-_{n+1/2} &= e^{\frac{i}{2}\tau\Delta} z_n; \\ z^+_{n+1/2} &= \exp\left(-i\tau\left(|w^-_{n+1/2}|^2+\Delta(|w^-_{n+1/2}|^2)\right)\right)\left(Id-i\tau\tilde{H}_{w^-_{n+1/2}}\right) z^-_{n+1/2}; \\ z_{n+1} &= e^{\frac{i}{2}\tau\Delta} z^+_{n+1/2}, \end{aligned} \tag{4.11}$$

where, taking $w^-_{n+1/2} = w_1+iw_2$, we have

$$\begin{aligned} \tilde{H}_{w^-_{n+1/2}} = &\begin{bmatrix} 2w_1w_2\Delta & 2w_2^2\Delta \\ -2w_1^2\Delta & -2w_1w_2\Delta \end{bmatrix} + \begin{bmatrix} 2w_2^2+2w_1w_2 & w_1^2+w_2^2 \\ -[3w_1^2+w_2^2] & -2w_1w_2 \end{bmatrix} \\ &+ \begin{bmatrix} 4w_2\nabla w_1\cdot\nabla & 4w_2\nabla_n w_2\cdot\nabla \\ -[4w_1\nabla w_1\cdot\nabla] & -[4w_1\nabla w_2\cdot\nabla] \end{bmatrix} \\ &+ \begin{bmatrix} 2w_2\Delta w_1 & \sum_{j=1}^2 2\nabla\cdot(w_j\nabla w_j)+2w_2\Delta w_2 \\ -\left[\sum_{j=1}^2 2\nabla\cdot(w_j\nabla w_j)+2w_1\Delta w_1\right] & -[2w_1\Delta w_2] \end{bmatrix}. \end{aligned}$$

To address the linear stability of the Strang splitting scheme, consider a linearly unstable mode corresponding to (4.10) such that z is regular. The linearized splitting scheme to the leading order works as

$$\begin{aligned} z^-_{n+1/2} &= \left(Id+\frac{1}{2}\begin{pmatrix} & -\tau\Delta \\ \tau\Delta & 0 \end{pmatrix}\right) z_n; \\ z^+_{n+1/2} &= \left(Id+\tau\begin{pmatrix} 2w_1w_2\Delta_n & 2w_2^2\Delta_n \\ -2w_1^2\Delta_n & -2w_1w_2\Delta_n \end{pmatrix}\right) z^-_{n+1/2}; \\ z_{n+1} &= \left(Id+\frac{1}{2}\begin{pmatrix} & -\tau\Delta \\ \tau\Delta & 0 \end{pmatrix}\right) z^+_{n+1/2}, \end{aligned} \tag{4.12}$$

and hence

$$z_{n+1} = z_n+\tau\begin{pmatrix} 2w_1w_2\Delta & (2w_2^2-1)\Delta \\ (1-2w_1^2)\Delta & -2w_1w_2\Delta \end{pmatrix} z_n+\mathcal{O}(\tau^2). \tag{4.13}$$

As a result, if w_1 and w_2 are constant (which we can assume only locally with any accuracy) and $2|w|^2-1>0$, we observe that each Fourier mode $z_{n+1,k}$ can be approximated by the linearized dynamical system

$$z_{n+1,k} = z_{n,k}+\tau\begin{pmatrix} -2w_1w_2k^2 & -(2w_2^2-1)k^2 \\ (2w_1^2-1)k^2 & 2w_1w_2k^2 \end{pmatrix} z_{n,k} \tag{4.14}$$

which has eigenvalues $1\pm\tau k^2\sqrt{2|w|^2-1}$ and hence would clearly grow exponentially for $|w|>\sqrt{2}/2$. For sufficiently large k, we observe that all the Fourier modes of w_1 and w_2 are small perturbations and hence exponential growth will occur just as in the backwards heat flow generated from the continuous approximation. Indeed, for τ sufficiently small, we have that the linearized Strang splitting flow well approximates the unstable backwards heat flow and hence displays linear instability. However, of course, the nonlinear effects are ignored in this computation.

To make this more precise, we observe from [40] that for the full PDE model (1.3) we can construct initial data for (1.4) having L^∞ norm larger than $\sqrt{2}/2$ but sufficiently localized in frequency such that the solution exists locally in time. A simple example of a solution with a global existence time and initial L^∞ norm larger than $\sqrt{2}/2$ is an exact plane-wave solution for the periodic problem. However, perturbations of such exact solutions are still linearly unstable as calculated in Section 4.1. The backward heat equation that represents the linearization of the continuous model exists locally in time when considering frequency localized data; however, this time scale will depend on the frequency cut-off and potentially be quite short given the nonlinear interactions. Using Theorem 3.1, we observe that in the semi-discretized equation choosing $\tau\ll 1$ sufficiently small compared to the scale of local existence for (1.4), the numerical solution computed using the Strang splitting scheme is $\mathcal{O}(\tau^2)$ provided the solution is sufficiently regular. Of course, from (4.13), on a single time-step, the Strang splitting solution has a polynomial instability. However, the linearized equations in (4.10) give exponential growth dynamics for the full solution on the time scale of local existence. Since, on the scale of existence, the numerical solution remains $\mathcal{O}(\tau^2)$, the linear instability is inherited by the numerical solution over repeated iterations of the time step.

5. Regularity of the Time Evolution

In the analysis of the convergence of the Strang splitting scheme, we have used the analyticity of the linear Schrödinger evolution. However, this is not the case in general for the quasilinear Schrödinger evolution. The Strang splitting scheme actually regularizes the time flow of the original PDE. In this section, we give some further discussion for the regularity of the time evolution.

Let us show that the solution map of a quasilinear Schrödinger evolution is continuous in time for (1.1). The continuity partially hinges upon the proof of uniqueness for the evolution. In particular, take two solutions to a more general quasilinear model of the form (1.2), say u_1 and u_2. Setting $v=u_1-u_2$ and linearizing, we have an equation of the form

$$\begin{cases} iv_t+a^{jk}(u)\partial_j\partial_k v+V\nabla v+Wv=0,\\ v(0,x)=u_1(0)-u_2(0) \end{cases}$$

with

$$V=V(u_1,\nabla u_1,u_2,\nabla u_2),\quad W=h(u_1,\nabla u_1,u_2,\nabla u_2)+g(u_1,u_2)\nabla^2 u_1$$

for functions V, h, and g related to the Taylor expansion of the metric and the nonlinearity. Then, to solve this linear equation, we use [40, Proposition 5.1] (see also [39, Proposition 5.2]) to show that the weak Lipschitz bound

$$\|v\|_{L^\infty H^\sigma}\lesssim\|v(0)\|_{H^\sigma} \tag{5.1}$$

holds for any $0\le\sigma\le s-1$ via energy estimates on the linearized equation where we recall that the initial condition lies in H^s for $s>\frac{d+5}{2}$. However, in the well-posedness

result for the linearized version of (1.1) (see Proposition 5.1 of [40], for instance), we have at most continuity of the solution map with respect to time in the H^s norm.

The key ideas of the proof follow from the theory of frequency envelopes as discussed in both [39, 40, Sections 2 and 5] where it is proven that the size of a dyadic frequency component of the solution to (1.1) in a natural energy space is bounded by a uniform constant times the corresponding dyadic frequency component of the initial data in H^s. To be more precise, we shall use a Littlewood-Paley decomposition of the spatial frequencies,

$$\sum_{i=0}^{\infty} S_i(D) = 1,$$

where S_i localizes to frequency $|\xi| \in [2^{i-1}, 2^{i+1}]$ for $i > 0$ and to frequencies $|\xi| \leq 2$ for $i = 0$. By a frequency envelope, we recall from [39, Section 2.4] that we mean that given a translation invariant space U such that

$$\|u\|_U^2 \sim \sum_{k=0}^{\infty} \|S_k u\|_U^2,$$

a frequency envelope for u in U is a positive sequence a_j so that

$$\|S_j u\|_U \leq a_j \|u\|_U, \qquad \sum a_j^2 \approx 1. \tag{5.2}$$

We say that a frequency envelope is admissible if $a_0 \approx 1$ and it is slowly varying,

$$a_j \leq 2^{\delta |j-k|} a_k, \qquad j,k \geq 0, \qquad 0 < \delta \ll 1.$$

An admissible frequency envelope always exists, say by

$$a_j = 2^{-\delta j} + \|u\|_U^{-1} \max_k 2^{-\delta |j-k|} \|S_k u\|_U. \tag{5.3}$$

Abusing notation and avoiding for simplicity the atomic space formulations in [39, 40], we rely upon a uniform bound over the evolution such that effectively

$$\|u\|_{L^\infty H^s} \lesssim \|u_0\|_{H^s}. \tag{5.4}$$

We note that the $L^\infty H^s$ norm appearing in the estimate here is due to the cubic interactions in the nonlinearity and the compactness of our domain, otherwise one must enforce further summability as in [39]. A key estimate is the following proposition.

PROPOSITION 5.1 (Proposition 5.3, [39]; Proposition 5.4, [40]). *Let u be a small data solution to* (1.1) *which satisfies* (5.4). *Let $\{a_j\}$ be an admissible frequency envelope for the initial data u_0 in H^s. Then $\{a_j\}$ is also a frequency envelope for u in $L^\infty H^s$.*

Once we have Proposition 5.1, the continuity of the solution map can be established as in Section 5.7 of [39]. Namely, we consider a sequence of initial data $\{u_0^n\} \to u_0$ in H^s. Frequency envelope bounds can then be chosen such that there exists a uniform N_ϵ for which

$$\|a_{N_\epsilon}^{(n)}\| \leq \epsilon$$

for all n, which gives a uniform upper bound by Proposition 5.1 on the high frequencies of each corresponding solution $u^{(n)}$ to (1.1) with initial data $u_0^{(n)}$ in the $L^\infty H^s$ norm.

Separating into low and high frequencies and using the smallness of the high frequencies and the uniform convergence in weaker Sobolev norms provided by (5.1), the result follows.

Let us emphasize, however, that we generally gain no more than continuity of the solution map from such arguments. Hence, in order to accurately compare the flow of the full solution map defined by (1.1) and that of the Strang splitting method, we rely on differentiating the equation and the balancing of spatial and time regularity as in Section 3.

6. Convergence of the Pseudospectral Flow

In this section, we address the closeness of the flow from the continuous equation to a mollified equation representing the effects of a full pseudo-spectral discretization scheme. Namely, we take

$$iu_{\epsilon,t}+u_{\epsilon,xx}=G_\epsilon*[|u_\epsilon|^2u_\epsilon]+G_\epsilon*[\Delta(|u_\epsilon|^2)u_\epsilon] \tag{6.1}$$

for $G_\epsilon\in C_c^\infty$ a smooth, compactly supported mollifier such that if $u\in H^s$ we have

$$\|G_\epsilon u-u\|_{H^{s-1}}\leq C\epsilon\|u\|_{H^s}$$

as $\varepsilon\to 0$. Note, this is essentially an exponentially decaying cut-off in frequency space $S_{<N_\epsilon}$ for $N_\epsilon=\mathcal{O}(1/\epsilon)$. We wish to compare this to the evolution of (2.1).

PROPOSITION 6.1. *For $\|u_0\|_{H^s}\ll 1$ sufficiently small with $s>3$, (6.1) has a solution that exists for time 1 and remains sufficiently small. In addition, if u solves (2.1) we have $\|u-u_\epsilon\|_{L^\infty([0,1]\times H^\sigma)}=\mathcal{O}(\epsilon)$ as $\epsilon\to 0$ for all $\sigma<s-3$.*

Proof. Intuitively, we rely on the paradifferential scheme providing the frequency envelope bounds of [40] which states that, at least for small enough data with enough regularity, on time 1 intervals the high frequencies do not change the flow very much. In particular, we use the fact that the flow of both equations is well-defined in H^s for $s>\frac{d+5}{2}$.

Let us, for the sake of completeness, briefly review paradifferential estimates from [40]. We are interested for our particular numerical purposes in (1.1), but, since the results are also true in higher dimensions, let us work with a more general quasilinear equation of the form (1.2). We use a Picard iteration scheme to boil down finding a solution to solving the linear problem

$$\begin{cases}(i\partial_t+\partial_k a^{kl}(w)\partial_l)u+V\nabla u+Wu=H,\\ u(0)=u_0\end{cases} \tag{6.2}$$

and

$$\begin{cases}(i\partial_t+\partial_k a^{kl}(w)\partial_l)u+V\nabla u=H,\\ u(0)=u_0\end{cases} \tag{6.3}$$

under the assumption that

$$g^{kl}-\delta^{kl}=h^{kl}(w(t,x)),$$

where $h(z)=O(|z|^2)$ near $|z|=0$ with w a small function in an energy space and H a generic forcing term that is small in the dual to that energy space at the moment. We include H so that the error term from frequency cut-offs can be included below.

We want to use a paradifferential scheme such that u_j at frequency j solves

$$\begin{cases} (i\partial_t + \partial_k a^{kl}_{<j-4}\partial_l)u_j = G_j + H_j, \\ u_j(0) = u_{0j}, \end{cases}$$

where $a^{kl}_{<j-4} = S_{<j-4}a^{kl}$ is cut-off to slightly lower frequencies, and hence

$$G_j = -S_j\partial_k g^{kl}_{>j-4}\partial_l u - [S_j, \partial_k g^{kl}_{<j-4}\partial_l]u - S_j V\nabla u - S_j W u.$$

Then, we construct a full solution by summing over frequency.

Applying the general energy estimates from Proposition 4.1 to each of these equations, we see that

$$\|u\|^2_{l^2X^\sigma} \lesssim \|u_0\|^2_{H^\sigma} + \|H\|^2_{l^2Y^\sigma} + \sum_j \|G_j\|^2_{l^2Y^\sigma}.$$

If $W = 0$, we can take $\sigma = s$, otherwise we work with $\sigma = s-1$. However, these estimates are strong enough to give a bootstrapping argument. The spaces l^2X^σ, l^2Y^σ here require using smoothing properties of the linear Schrödinger equation and will not be discussed in detail here. See [40] for more details on their construction.

Convergence estimates in Sobolev spaces follows directly from energy estimates for the truncated equation and the frequency envelope analysis in Section 5 on solutions to (2.1). Note that we make no claims that our convergence estimates for the pseudospectral scheme are sharp, and, in fact, being more careful with convergence estimates above might improve future results. Since we are largely worried about the L^2 and H^1 convergence, there is a relatively simple approach inspired by Propositions 5.1 and 5.2 from [40] that gives a frequency envelope decomposition for the solution u of (2.1). We observe

$$\begin{aligned} \|u - u_\epsilon\|_{L^\infty([0,1]\times H^\sigma)} \leq C\big(&\|(1-G_\epsilon)u_0\|_{H^\sigma} + \||u|^2u - G_\epsilon(|G_\epsilon u|^2 G_\epsilon u)\|_{H^\sigma} \\ &+ \|(|u|^2)_{xx}u - G_\epsilon((|G_\epsilon u|^2)_{xx}G_\epsilon u)\|_{H^\sigma}\big) \\ \leq C(&\|u\|_{L^\infty H^{\sigma+3}})\epsilon, \end{aligned}$$

where we have emphasized the dependence on the constant in the final inequality on $\|u\|_{L^\infty H^{\sigma+3}}$. The convergence is easily controlled using the frequency envelopes of u, and hence the nonlinear expressions of u, using that $s > d/2$ and the smallness of u. As a result, if the initial datum has a small $\|\cdot\|_{H^{\sigma+3}}$ norm, $\|u\|_{L^\infty H^{\sigma+3}}$ is controlled and hence so is the difference between u and u_ϵ. □

7. Conclusion

In this work, we have studied the Strang splitting scheme for quasilinear nonlinear Schrödinger equations. The splitting scheme is proved to have second order convergence for small data. We further investigate the regularity of the time flow and the instability of the numerical scheme which leads to numerically observed blow-ups.

Our work is motivated by numerical approaches towards time-dependent density functional theory computations as discussed in the documentation of the software package Octopus [1, 13] and references therein. The mathematical analysis and numerical schemes for time-dependent density functional theory will be an exciting direction to explore in the future.

REFERENCES

[1] X. Andrade, J. Alberdi-Rodriguez, D. A. Strubbe, M. J. T. Oliveira, F. Nogueira, A. Castro, J. Muguerza, A. Arruabarrena, S. G. Louie, A. Aspuru-Guzik, A. Rubio, and M. A. L. Marques, *Time-dependent density-functional theory in massively parallel computer architectures: the octopus project*, J. Phys.: Cond. Matt. 24, 233202, 2012.

[2] G.D. Akrivis, V.A. Dougalis, O.A. Karakashian, and W.R. McKinney, *Numerical approximation of blow-up of radially symmetric solutions of the nonlinear Schrödinger equation*, SIAM J. Sci. Comput., 25(1), 186–212, 2003.

[3] D. Ambrose and G. Simpson, *Local existence theory for derivative nonlinear Schrödinger equations with non-integer power nonlinearities*, preprint available at arXiv:1401.7060, 2014.

[4] X. Antoine, W. Bao, and C. Besse, *Computational methods for the dynamics of the nonlinear Schrödinger/Gross–Pitaevskii equations*, Comput. Phys. Commun., 184(12), 2621–2633, 2013.

[5] H. Appel and E.K.U. Gross, *Static and time-dependent many-body effects via density-functional theory*, Quantum Simulations of Complex Many-Body Systems: From Theory to Algorithms, John von Neumann Institute for Computing Press NIC Series, 10, 255–268, 2002.

[6] U.M. Ascher, S.J. Ruuth, and B.T.R. Wetton, *Implicit-explicit methods for time-dependent partial differential equations*, SIAM. J. Numer. Anal., 32, 797–823, 1995.

[7] W. Bao and Y. Cai, *Mathematical theory and numerical methods for Bose–Einstein condensation*, Kinet. Relat. Models, 6(1), 1–135, 2013.

[8] W. Bao, D. Jaksch, and P.A. Markowich, *Numerical solution of the Gross–Pitaevskii equation for Bose–Einstein condensation*, J. Comput. Phys., 187, 318–342, 2003.

[9] W. Bao, S. Jin, and P.A. Markowich, *Numerical study of time-splitting spectral discretizations of nonlinear Schrödinger equations in the semiclassical regimes*, SIAM J. Sci. Comput., 25, 27–64, 2003.

[10] W. Bao, N. Mauser, and H.P. Stimming, *Effective one particle quantum dynamics of electrons: a numerical study of the Schrödinger–Poisson-Xα model*, Commun. Math. Sci., 1, 809–828, 2003.

[11] W. Bao and J. Shen, *A fourth-order time-splitting Laguerre–Hermite pseudospectral method for Bose–Einstein condensates*, SIAM J. Sci. Comput., 26, 2010–2028, 2005.

[12] S. Blanes, F. Casas, J.A. Oteo, and J. Ros, *The Magnus expansion and some of its applications*, Phys. Rep., 470, 151–238, 2009.

[13] A. Castro, M.A.L. Marques, and A. Rubio, *Propagators for the time-dependent Kohn–Sham equations*, J. Chem. Phys., 121(8), 3425–3433, 2004.

[14] S.A. Chin, *Higher-order splitting algorithms for solving the nonlinear Schrödinger equation and their instabilities*, Phys. Rev. E, 76, 056708, 2007.

[15] S.M. Cox and P.C. Matthews, *Exponential time differencing for stiff systems*, J. Comput. Phys., 176, 430–455, 2002.

[16] A. De Bouard, N. Hayashi, and J.C. Saut, *Global existence of small solutions to a relativistic nonlinear Schrödinger equation*, Comm. Math. Phys., 189, 73–105, 1997.

[17] A. De Bouard, N. Hayashi, P.I. Naumkin, and J.C. Saut, *Scattering problem and asymptotics for a relativistic nonlinear Schrödinger equation*, Nonlinearity, 12, 1415–1425, 1999.

[18] S. Descombes and M. Thalhammer, *The Lie–Trotter splitting for nonlinear evolutionary problems with critical parameters: a compact local error representation and application to nonlinear Schrödinger equations in the semiclassical regime*, IMA J. Numer. Anal., 33, 722–745, 2013.

[19] E. Faou, V. Gradinaru, and C. Lubich, *Computing semiclassical quantum dynamics with Hagedorn wavepackets*, SIAM J. Sci. Comput., 31, 3027–3041, 2009.

[20] L. Gauckler, *Convergence of a split-step Hermite method for the Gross–Pitaevskii equation*, IMA J. Numer. Anal., 31, 396–415, 2011.

[21] R.H. Hardin and F.D. Tappert, *Applications of the split-step Fourier method to the numerical solution of nonlinear and variable coefficient wave equations*, SIAM Rev. 15, 423, 1973.

[22] H. Hofstätter, O. Koch, and M. Thalhammer, *Convergence analysis of high-order time-splitting pseudo-spectral methods for rotational Gross–Pitaevskii equations*, Numer. Math., 127(2), 315–364, 2014.

[23] H. Holden, C. Lubich, and N.H. Risebro, *Operator splitting for partial differential equations with Burgers nonlinearity*, Math. Comp., 82(281), 173–185, 2013.

[24] J. Holmer, J. Marzuola, and M. Zworski, *Soliton splitting by external delta potentials*, J. Nonlinear Sci., 17(4), 349–367, 2007.

[25] T. Jahnke and C. Lubich, *Error bounds for exponential operator splittings*, BIT, 40, 735–744, 2000.

[26] S. Jin, *Schrödinger equation: Computation*, Encyclopedia of Applied and Computational Mathematics, B. Engquist (ed.), to appear.
[27] S. Jin, P.A. Markowich, and C. Sparber, *Mathematical and computational methods for semiclassical Schrödinger equations*, Acta Numer., 20, 121–209, 2011.
[28] A.K. Kassam and L.N. Trefethen, *Fourth-order time-stepping for stiff PDEs*, SIAM J. Sci. Comput., 26, 1214–1233, 2005.
[29] C.E. Kenig, G. Ponce, and L. Vega, *Small solutions to nonlinear Schrödinger equations*, Ann. Inst. H. Poincaré Anal. Non Linéaire, 10, 255–288, 1993.
[30] C.E. Kenig, G. Ponce, and L. Vega, *Smoothing effects and local existence theory for the generalized nonlinear Schrödinger equations*, Invent. Math., 134, 489–545, 1998.
[31] C.E. Kenig, G. Ponce, and L. Vega, *The Cauchy problem for quasi-linear Schrödinger equations*, Invent. Math., 158, 343–388, 2004.
[32] C.E. Kenig, G. Ponce, C. Rolvung, and L. Vega, *The general quasilinear ultrahyperbolic Schrödinger equation*, Adv. Math., 206(2), 402–433, 2006.
[33] C.E. Kenig, G. Ponce, C. Rolvung, and L. Vega, *Variable coefficient Schrödinger flows for ultrahyperbolic operators*, Adv. Math., 196(2), 373–486, 2005.
[34] R. Krasny, *A study of singularity formation in a vortex sheet by the point-vortex approximation*, J. Fluid Mech., 167, 65–93, 1986.
[35] S. Kurihara, *Large-amplitude quasi-solitons in superfluid films*, J. Phys. Soc. Japan, 50, 3262–3267, 1981.
[36] H. Lange, M. Poppenberg, and H. Teismann, *Nash–Moser methods for the solution of quasilinear Schrödinger equations*, Comm. Part. Diff. Eqs., 24(7-8), 1399–1418, 1999.
[37] C. Lubich, *On splitting methods for Schrödinger-Poisson and cubic nonlinear Schrödinger equations*, Math. Comp., 77(264), 2141–2153, 2008.
[38] W. Magnus, *On the exponential solution of differential equations for a linear operator*, Comm. Pure Appl. Math., 7, 649–673, 1954.
[39] J. Marzuola, J. Metcalfe, and D. Tataru, *Quasilinear Schrödinger equations I: Small data and quadratic interactions*, Adv. Math., 231(2), 1151–1172, 2012.
[40] J. Marzuola, J. Metcalfe, and D. Tataru, *Quasilinear Schrödinger equations II: Small data and cubic nonlinearities*, Kyoto J. Math., 54(3), 529–546, 2014.
[41] R.I. McLachlan and G.R.W. Quispel, *Splitting methods*, Acta Numer., 11, 341–434, 2002.
[42] D. Pathria and J.L. Morris, *Pseudo-spectral solution of nonlinear Schrödinger equations*, J. Comput. Phys., 87, 108–125, 1990.
[43] V.M. Pérez-García and X. Liu, *Numerical methods for the simulation of trapped nonlinear Schrödinger systems*, Appl. Math. Comput., 144, 215–235, 2003.
[44] M. Poppenberg, *On the local well posedness of quasilinear Schrödinger equations in arbitrary space dimension*, J. Diff. Eqs., 172, 83–115, 2001.
[45] J.M. Sanz-Serna, *Methods for the numerical solution of the nonlinear Schrödinger equation*, Math. Comp., 43, 21–27, 1984.
[46] J. Shen and Z.Q. Wang, *Error analysis of the Strang time-splitting Laguerre–Hermite/Hermite collocation methods for the Gross–Pitaevskii equation*, Found. Comput. Math., 13(1), 99–137, 2013.
[47] G. Strang, *On the construction and comparison of difference schemes*, SIAM J. Numer. Anal., 5, 506–517, 1968.
[48] M. Suzuki, *Improved Trotter-like formula*, Phys. Lett. A, 180, 232–234, 1993.
[49] T.R. Taha and M.J. Ablowitz, *Analytical and numerical aspects of certain nonlinear evolution equations. II. Numerical, nonlinear Schrödinger equation*, J. Comput. Phys., 55, 203–230, 1984.
[50] M. Thalhammer, *High-order exponential operator splitting methods for time-dependent Schrödinger equations*, SIAM J. Numer. Anal., 46, 2022–2038, 2008.
[51] M. Thalhammer, *Convergence analysis of high-order time-splitting pseudospectral methods for nonlinear Schrödinger equations*, SIAM J. Numer. Anal., 50(6), 3231–3258, 2012.
[52] J.A.C. Weideman and B.M. Herbst, *Split-step methods for the solution of the nonlinear Schrödinger equation*, SIAM J. Numer. Anal., 23, 485–507, 1986.
[53] H. Yoshida, *Construction of higher order symplectic integrators*, Phys. Lett. A, 150, 262–268, 1990.